Research Article | Vol. 29, No. 9 / 26 April 2021 / Optics Express 13552
Optics EXPRESS

Ranging and velocimetry measurements by phase-based MTCW lidar

MUSTAFA MERT BAYER* AND OZDAL BOYRAZ

Electrical Engineering and Computer Science Department, University of California, Irvine, CA 92697, USA
*bayerm@uci.edu

Abstract: We propose a complementary phase detection algorithm to enhance the capabilities of the multi-tone continuous wave (MTCW) lidar for single-shot simultaneous ranging and velocimetry measurements. We show that the phase of the Doppler-shifted RF tones and the amount of the induced Doppler frequency shift can be used to extract the phase and velocity information, simultaneously. A numerical case study and experimental work have been performed for the proof of concept. We show that the velocity resolutions are limited by frequency resolution and the ranging resolution is determined by the temporal resolution. Experimentally, we obtain 8.08 ± 0.8cm/s velocity measurement and 111.9cm range measurements with ± 0.75cm resolution in a 6-tone MTCW lidar system.

1. Introduction

The light detection and ranging (lidar) market is rapidly growing over the past years [1] and the lidar industry is always hungry for new developments in various fields such as autonomous vehicles [2], airborne lidars for terrestrial applications [3], spacecraft [4], and precision measurements [5]. The pulse time-of-flight (PToF) is the most common technique that provides a robust ranging methodology by taking advantage of high peak power pulsed light sources and conventional direct detection methods [6]. However, simultaneous ranging and velocimetry of a moving target are not achievable via PToF lidars without generating and comparing multiple frames of the environment with respect to time [7–9], or without renewing the PToF methodology with enhanced configurations [10]. On the other hand, lidars operating in the continuous wave (CW) mode can perform coherent light detection to extract high-resolution single-shot range and velocity information of dynamic targets [11–14]. In particular, frequency-modulated continuous-wave (FMCW) lidars operate by linearly sweeping the frequency of a CW laser and using the interference of the delayed backscattering signal with the local oscillator to produce a beating note, which corresponds to the target distance [15]. By employing triangular waveform frequency modulation, FMCW lidars can yield the Doppler shifts induced by target velocity, simultaneously [10]. Even though the FMCW lidars can perform single shot ranging and velocimetry, the performance of the measurement highly depends on the scan duration, linearity of the frequency sweep, and frequency span that the source scans [14–16]. Eventually, the type of application and the required measurements, cost of the system, and resolution requirements dictate the type of the lidar suitable for the given application.

As an alternative to the current lidar technologies, we have previously introduced the multi-tone continuous wave (MTCW) lidar that operates in CW mode and eliminates the need for frequency sweeping [17–21]. The MTCW lidar utilizes the different phase shifts acquired by static radiofrequency (RF) tones imposed on the CW carrier. In particular, the coherent detection at the receiver end converts these frequency-dependent phase shifts into amplitude variations at RF tones; hence, allows us to predict the range of the target from these amplitude variations in a single shot measurement [18,19]. The ranging resolution of the system is determined by the span of the static RF tones and signal-to-noise ratio (SNR) at the receiver. Since there is no need for frequency, phase, or amplitude sweeping, it is suitable for conventional off-the-shelf light sources.

#422710 https://doi.org/10.1364/OE.422710
Journal © 2021 Received 15 Feb 2021; revised 4 Apr 2021; accepted 7 Apr 2021; published 19 Apr 2021

Optics EXPRESS

We have already demonstrated the static target ranging via the MTCW lidar [17,18], as well as the ranging of slow-moving targets [19]. However, the simultaneous ranging and velocimetry measurements are affected by the speed of the target in the MTCW lidar, because the desired interference diminishes and new RF beating tones appear if the resultant Doppler shifts are bigger than the optical carrier linewidth. Since the coherence length of the light is determined by the linewidth of the laser, and narrow linewidth lasers are compulsory for long-range applications, the MTCW methodology should be enhanced to address the Doppler shifts caused by the moving targets with arbitrary velocities in practice [19]. Also, the amplitude variations are sensitive to the relative signal amplitudes at the reference arm and the collection arm.

In this manuscript, we propose a complementary phase detection algorithm to enhance the capabilities of the MTCW lidar for single-shot simultaneous ranging and velocimetry measurements. As described in the original MTCW approach [17–19], the range information of the target is stored in the phases of the individual RF tones. Here, we show that instead of focusing on the amplitude variations, the phase of the Doppler-shifted RF tones and the amount of the induced Doppler frequency shift can be used to extract the range and velocity information, simultaneously. Specifically, we present the distribution of tones, their phases, and the amplitude information, and how we can utilize these to enhance the single-shot measurements. Combined with quasi-CW signals that facilitate coarse PToF measurements, the proposed technique can give high resolution ranging limited by the maximum tone frequency and temporal resolution of detection electronics irrespective of the target distance. The resolution can be further enhanced by using prediction algorithms [22]. Moreover, the proposed approach has the potential to mitigate the requirement for a narrow linewidth laser for coherent detection, since we use the relative phase changes of RF tones instead of absolute phase and frequency measurements as a means to determine the target range. Furthermore, this technique eliminates the power-balance requirements in between the local oscillator and the echo signal, which forced the system to have an integrated monitoring photodetector and a variable attenuator to realize the power balance [19]. To prove the concept, a simple case study on simultaneous ranging and velocimetry of a fast dynamic target is performed via numerical simulations. We show that a $<\pm$1cm resolution in the ranging, limited by the temporal resolution of the detection system, and a 0.4cm/s speed resolution that is limited by the linewidth of the laser and frequency resolution of the detection system are achievable. Furthermore, experimental results are presented to demonstrate the capability of the proposed methodology.

2. Theoretical modelling

The schematic of the MTCW lidar for fast target ranging and velocimetry is presented in Fig. 1. A narrow linewidth CW laser with an output electric field of E_1 is modulated via a balanced Mach-Zehnder modulator (MZM) under push-pull configuration. Multiple RF tones, f_i, with the same initial phases are fed to the MZM that yields optical field, E_2, at the output facet of the collimator (CL). The modulator is configured to have a linear modulation with a low modulation depth of $m<<1$ [18] and the corresponding E_2 is shown in Eq. (1).

$$E_2 = \frac{A_0}{\sqrt{2}} exp(j\omega_0 t + j\phi_0) - \frac{mA_0}{4\sqrt{2}} \sum_{i=1}^{N} (exp[j(\omega_0 + \omega_i)t + j(\phi_0 + \phi_i)] + exp[j(\omega_0 - \omega_i)t + j(\phi_0 - \phi_i)]) \tag{1}$$

Here, A_0, ω_0, and ϕ_0 represent the electric field amplitude, angular optical carrier frequency, and the initial phase of the CW laser, respectively. Similarly, ω_i indicates the angular frequency of i^{th} RF modulation tone, and ϕ_i is the initial phase of the corresponding tone.

The laser beam is then split into two via a beamsplitter (BS), where one arm is kept as the local oscillator and the other as the measurement branch to realize coherent detection on the photodetector (PD). The local signal is transmitted to the reference mirror that is separated from the BS by a distance L_{ref}. The back-reflected signal from the reference mirror accumulates a

Optics EXPRESS

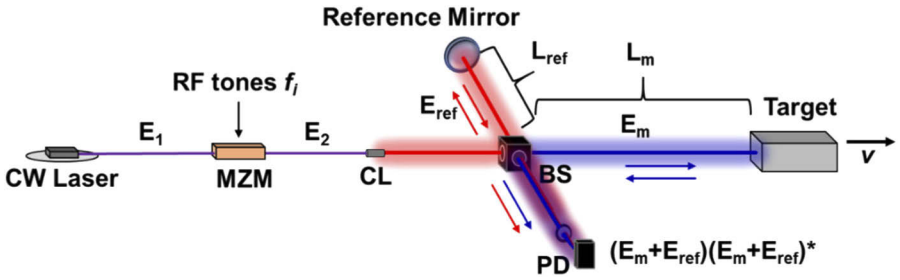

Fig. 1. Schematic of the MTCW lidar that consists of a narrow linewidth CW laser, Mach-Zehnder modulator (MZM), collimator (CL), beamsplitter (BS), reference mirror, and photodetector (PD). The target and reference distances are labeled as L_m and L_{ref}, respectively.

phase with respect to the corresponding frequency and has the field equation E_{ref} as given in Eq. (2), where α_{ref} is the linear attenuation coefficient realized in the reference arm and c is the speed of light.

$$E_{ref} = \frac{A_0}{2\sqrt{2}}\alpha_{ref} exp(j\omega_0 t + j\omega_0 \frac{2L_{ref}}{c} + j\phi_0) - \frac{mA_0}{4\sqrt{2}}\alpha_{ref} \sum_{i=1}^{N} \left(exp\left[j(\omega_0+\omega_i)t + j(\omega_0+\omega_i)\frac{2L_{ref}}{c} + j(\phi_0+\phi_i)\right] + exp\left[j(\omega_0-\omega_i)t + j(\omega_0-\omega_i)\frac{2L_{ref}}{c} + j(\phi_0-\phi_i)\right]\right) \quad (2)$$

The electric field in the measurement branch is represented by E_m, where the target speed, v, alters the echo signal by inducing Doppler shift, ω_d, to the optical carrier frequency by $\omega_d = (2v/c)\omega_0$ after the laser beam travels a distance of L_m [23,24]. Similarly, each modulation frequency realizes a Doppler shift of ω_d^i, as well. The returned signal electric field equation after the completion of the round trip is shown in Eq.(3).

$$E_m = \frac{A_0}{2\sqrt{2}}\alpha_m exp(j(\omega_0+\omega_d)t + j\omega_0\frac{L_m}{c} + j(\omega_0+\omega_d)\frac{L_m}{c} + j\phi_0) - \frac{mA_0}{4\sqrt{2}}\alpha_m \sum_{i=1}^{N} \left(\begin{array}{l} exp\left[j(\omega_0+\omega_i+\omega_d+\omega_d^i)t + j(\omega_0+\omega_i)\frac{L_m}{c} + j(\omega_0+\omega_i+\omega_d+\omega_d^i)\frac{L_m}{c} + j(\phi_0+\phi_i)\right] \\ +exp\left[j(\omega_0-\omega_i+\omega_d-\omega_d^i)t + j(\omega_0-\omega_i)\frac{L_m}{c} + j(\omega_0-\omega_i+\omega_d-\omega_d^i)\frac{L_m}{c} + j(\phi_0-\phi_i)\right] \end{array} \right) \quad (3)$$

The forward propagating and backscattered light have different phases due to change in the carrier and modulation frequencies. Since $\omega_0 >> \omega_i$, it is possible to assume $\omega_d + \omega_d^i \simeq \omega_d - \omega_d^i \simeq \omega_d$. Unless the laser linewidth is in the order of kHz or below and the target is moving at extreme velocities, this assumption is always true for most practical applications. The Doppler shift realized by individual modulation frequencies will be in the < kHz levels even for very fast targets, while the optical carrier will realize MHz level shifts. On the other hand, to further simplify Eqs. (2) and (3), we assume all carriers and sidetones are in phase, thus $\phi_0 = \phi_i = 0$.

After the beams in both arms propagate back to the PD from the reference mirror and the target, the corresponding electric fields will be converted into the detector photocurrent as $I_{PD} = R(E_m + E_{ref}) \cdot (E_m + E_{ref})^*$ to realize coherent detection, where R is the responsivity of the PD in A/W. The final I_{PD} equation is given in Eq. (4), where A_{ref} and A_m stand for $A_{ref} = \frac{A_0\alpha_{ref}}{2\sqrt{2}}$ and $A_m = \frac{A_0\alpha_m}{2\sqrt{2}}$, respectively. Moreover, selecting tone frequencies in a manner that prevents frequency overlap between desired beating tones and weak cross beating tones would improve the crosstalk and spur-free dynamic range of the measurement. For simplicity, the weak intermodulation terms between individual tone frequencies are neglected in Eq. (4). The expected spectral peaks in the frequency domain are stationed at ω_d, ω_i, $2\omega_i$, $\omega_i+\omega_d$, $\omega_i-\omega_d$, $2\omega_i+\omega_d$ and $2\omega_i-\omega_d$, and at their negatives if a dual side-band modulation is used. The phases of ω_i and $2\omega_i$ terms are highly dependent on the reference field and have a very small contribution from the measurement arm for a highly unbalanced system. However, in our previous MTCW experiments, we had demonstrated how to utilize those tones for range measurements by comparing the relative

Optics EXPRESS

amplitude variations [18,19].

$$
\begin{aligned}
I_{PD} &= RA_{ref}^2 + RA_m^2 + RA_{ref}A_m\left[exp\left(j\omega_d t + j\omega_d\frac{L_m}{c}\right) + exp\left(-j\omega_d t - j\omega_d\frac{L_m}{c}\right)\right] \\
&- mRA_{ref}^2\sum_{i=1}^{N}\left[exp\left(j\omega_i t + j\omega_i\frac{2L_{ref}}{c}\right) + exp\left(-j\omega_i t - j\omega_i\frac{2L_{ref}}{c}\right)\right] - mRA_m^2\sum_{i=1}^{N}\left[exp\left(j\omega_i t + j\omega_i\frac{2L_m}{c}\right) + exp\left(-j\omega_i t - j\omega_i\frac{2L_m}{c}\right)\right] \\
&+ \frac{m^2RA_{ref}^2}{4}\sum_{i=1}^{N}\left[2 + exp\left(j2\omega_i t + j\omega_i\frac{4L_{ref}}{c}\right) + exp\left(-j2\omega_i t - j\omega_i\frac{4L_{ref}}{c}\right)\right] \\
&+ \frac{m^2RA_m^2}{4}\sum_{i=1}^{N}\left[2 + exp\left(j2\omega_i t + j\omega_i\frac{4L_m}{c}\right) + exp\left(-j2\omega_i t - j\omega_i\frac{4L_m}{c}\right)\right] \\
&- \frac{mRA_mA_{ref}}{2}\sum_{i=1}^{N}\left[\begin{array}{l}
exp\left(j(\omega_i+\omega_d)t + j\left(\omega_i\frac{2L_{ref}}{c} + \omega_d\frac{L_m}{c}\right)\right) + exp\left(-j(\omega_i+\omega_d)t - j\left(\omega_i\frac{2L_{ref}}{c} + \omega_d\frac{L_m}{c}\right)\right) \\
+exp\left(j(\omega_i+\omega_d)t + j\left(\omega_i\frac{2L_m}{c} + \omega_d\frac{L_m}{c}\right)\right) + exp\left(-j(\omega_i+\omega_d)t - j\left(\omega_i\frac{2L_m}{c} + \omega_d\frac{L_m}{c}\right)\right) \\
+exp\left(j(\omega_i-\omega_d)t + j\left(\omega_i\frac{2L_{ref}}{c} - \omega_d\frac{L_m}{c}\right)\right) + exp\left(-j(\omega_i-\omega_d)t - j\left(\omega_i\frac{2L_{ref}}{c} - \omega_d\frac{L_m}{c}\right)\right) \\
+exp\left(j(\omega_i-\omega_d)t + j\left(\omega_i\frac{2L_m}{c} - \omega_d\frac{L_m}{c}\right)\right) + exp\left(-j(\omega_i-\omega_d)t - j\left(\omega_i\frac{2L_m}{c} - \omega_d\frac{L_m}{c}\right)\right)
\end{array}\right] \\
&+ \frac{m^2RA_mA_{ref}}{4}\sum_{i=1}^{N}\left[\begin{array}{l}
exp\left(j(2\omega_i+\omega_d)t + j\left(2\omega_i\left(\frac{L_m+L_{ref}}{c}\right) + \omega_d\frac{L_m}{c}\right)\right) + exp\left(-j(2\omega_i+\omega_d)t - j\left(2\omega_i\left(\frac{L_m+L_{ref}}{c}\right) + \omega_d\frac{L_m}{c}\right)\right) \\
+exp\left(j(2\omega_i-\omega_d)t + j\left(2\omega_i\left(\frac{L_m+L_{ref}}{c}\right) - \omega_d\frac{L_m}{c}\right)\right) + exp\left(-j(2\omega_i-\omega_d)t - j\left(2\omega_i\left(\frac{L_m+L_{ref}}{c}\right) - \omega_d\frac{L_m}{c}\right)\right) \\
+exp\left(j\omega_d t + j\left(2\omega_i\left(\frac{L_m-L_{ref}}{c}\right) + \omega_d\frac{L_m}{c}\right)\right) + exp\left(-j\omega_d t - j\left(2\omega_i\left(\frac{L_m-L_{ref}}{c}\right) + \omega_d\frac{L_m}{c}\right)\right) \\
+exp\left(j\omega_d t + j\left(2\omega_i\left(\frac{L_m-L_{ref}}{c}\right) + \omega_d\frac{L_m}{c}\right)\right) + exp\left(-j\omega_d t - j\left(2\omega_i\left(\frac{L_m-L_{ref}}{c}\right) + \omega_d\frac{L_m}{c}\right)\right)
\end{array}\right]
\end{aligned}
\tag{4}
$$

Equation (4) can be further simplified for tones at $\omega' = \omega_i \pm \omega_d$ or $\omega' = 2\omega_i \pm \omega_d$ as $4\cos\left(\frac{\phi'}{2} - \frac{\phi''}{2}\right)\cos\left(\omega' t + \frac{\phi'}{2} + \frac{\phi''}{2}\right)$by using trigonometric identities. The definitions of $\left(\frac{\phi'}{2} - \frac{\phi''}{2}\right)$ and $\left(\frac{\phi'}{2} + \frac{\phi''}{2}\right)$ for each tone are given in Table 1. Hence, their amplitudes and phases reveal the range information as indicated in Eq. (4) and Table 1. In particular, we focus on the phases of the measurable tones for the range information. Moreover, as shown in these definitions, for a system with N RF tones at the transmitter we have $4N$ frequency tones for data analysis for dynamic targets and we have $2N$ tones for static targets to extract the range information only, which is instrumental to increases the robustness and accuracy of the system. Here, we show an algorithm for single-shot range and velocity measurements by utilizing the phases rather than the tone amplitudes. For illustration purposes, we use the phase accumulations of tones at $\omega_i + \omega_d$ and $\omega_i - \omega_d$ only.

Table 1. Resultant frequencies and their corresponding amplitude, phase, and L_0 equations.

Frequency	Amplitude	Phase	$L_0^{\omega_i\pm\omega_d}$
$\omega_i + \omega_d$	$-4mRA_mA_{ref}\cos\left(\frac{\omega_i}{c}(L_m - L_{ref})\right)$	$\frac{\omega_i+\omega_d}{c}L_m + \frac{\omega_i}{c}L_{ref}$	$L_0^{\omega_i+\omega_d} = \frac{c\phi^{meas}_{\omega_i+\omega_d} - \omega_i L_{ref}}{\omega_i+\omega_d}$
$\omega_i - \omega_d$	$-4mRA_mA_{ref}\cos\left(\frac{\omega_i}{c}(L_m - L_{ref})\right)$	$\frac{\omega_i-\omega_d}{c}L_m + \frac{\omega_i}{c}L_{ref}$	$L_0^{\omega_i-\omega_d} = \frac{c\phi^{meas}_{\omega_i+\omega_d} - \omega_i L_{ref}}{\omega_i-\omega_d}$
$2\omega_i + \omega_d$	$\frac{m^2RA_mA_{ref}}{2}$	$\left(2\omega_i\left(\frac{L_m+L_{ref}}{c}\right) + \omega_d\frac{L_m}{c}\right)$	$L_0^{2\omega_i+\omega_d} = \frac{c\phi^{meas}_{2\omega_i+\omega_d} - 2\omega_i L_{ref}}{2\omega_i+\omega_d}$
$2\omega_i - \omega_d$	$\frac{m^2RA_mA_{ref}}{2}$	$\left(2\omega_i\left(\frac{L_m+L_{ref}}{c}\right) - \omega_d\frac{L_m}{c}\right)$	$L_0^{2\omega_i-\omega_d} = \frac{c\phi^{meas}_{2\omega_i+\omega_d} - 2\omega_i L_{ref}}{2\omega_i-\omega_d}$

One of the challenges in the proposed technique is the modulo 2π cyclic pattern of the phase accumulation. In other words, $\phi^{meas}_{\omega_i\pm\omega_d}$represents the measured phase of the indicated frequency term, where $0 \le \phi^{meas}_{\omega_i\pm\omega_d} \le 2\pi$, and yields the same phase result for every L_m such that inte$L_m = L_0^{\omega_i\pm\omega_d} + \frac{2\pi c}{\omega_i\pm\omega_d}n_i$, where n_i is an integer related with the i^{th} frequency and $L_0^{\omega_i\pm\omega_d}$is the measured length in the first cycle of the i^{th} frequency when $n_i = 0$. Therefore, we propose to use multiple tones to facilitate triangulation algorithms. In particular, if we define the integer $n_i = \left\lfloor\frac{L_m}{\lambda_{i-RF}}\right\rfloor$, where λ_{i-RF} is the RF tone wavelength, then we can define the possible measurement

Optics EXPRESS

distance L_m for a given phase measurement as in Eq. (5).

$$L_m = \frac{(2\pi n_i + \phi^{meas}_{\omega_i \pm \omega_d}) - \frac{\omega_i L_{ref}}{c}}{\frac{\omega_i \pm \omega_d}{c}} \tag{5}$$

Hence, for a given maximum measurable distance L_{m-max} that is determined by the system parameters, such as laser power, laser linewidth, SNR of the system, etc., we will have multiple solutions for the same target. While higher tone frequencies are desired for high resolution ranging, they are handicapped due to increasing n_i value. Lower frequency tones produce a lower number of solutions with coarser resolutions, whereas the rapidly varying phases on the higher frequency tones generate multiple solutions with higher resolutions. The actual ranging solution is a triangulation of all tone frequencies. One method of converging to a single solution after triangulation is selecting the lowest frequency RF tone such that $\lambda_{1-RF} \geq L_{m-\max}$. However, this will impose additional constraints on the detection electronics and the length of the time window that is utilized in the desired application. Similar to constraints in FMCW, if there is extensive scanning involved, using a longer time window will limit the number of scans that can be performed per second. Therefore, the number of RF tones and their frequency ranges should be determined based on the desired resolution and maximum ranging distance L_{m-max}. However, implementation of a pseudo pulsation or quasi-CW operation that uses long pulses with multi-tone RF modulations imposed on them can further enhance this approach by eliminating the limits of n_i described above and provide a higher SNR solution due to high peak power excitation.

Similar to FMCW lidars, the frequency variations due to Doppler shift are used to identify the velocity information [25]. We have up to $2N$ degrees of freedom to estimate the velocity information. The precision of the velocity measurement is determined by the time window used to capture the ranging. For instance, a 1ms time window will yield a 1kHz spectral resolution that corresponds to 1mm/s or 1.5mm/s resolutions in velocity measurements by using a $1\mu m$ laser or by using a standard telecom laser at $1.55\mu m$, respectively. The variations in Doppler shifts at different RF tones are negligibly small in most applications. For practical purposes, using tones with higher powers would yield high SNR velocity measurements. The value of ω_d can be extracted from the photocurrent spectrum by comparing the ω_i or $2\omega_i$ tones and its corresponding Doppler-shifted $\omega_i \pm \omega_d$ or $2\omega_i \pm \omega_d$ tones, respectively, or by evaluating the Doppler peak near the baseband.

3. Numerical verification

A numerical verification is performed by mimicking simultaneous ranging and velocimetry of a fast-moving target to demonstrate the system's capability. To configure the MTCW lidar, a narrow linewidth CW laser is set to operate at 1μm central wavelength. The laser beam enters the MZM with a selected modulation depth of $m = 0.01$ to maintain the linearity of the modulator. Four modulation frequencies are fed to the MZM at 75MHz, 500MHz, 1900MHz, and 2450MHz. These tones are carefully selected in a fashion to forestall any form of frequency overlapping over a $\omega_i \pm \omega_d$ frequency span. MZM output is followed by a beam splitter. At the detector, we assume that the reference signal amplitude is $\alpha_{ref} = 1$, while the signal from the target has an attenuation of $\alpha_m = 0.01$ pointing out a 20dB loss due to scattering.

The receiver is assumed to be an InGaAs PIN photodetector with a 5GHz bandwidth and 0.9A/W responsivity. The load impedance of the detector is set to 50Ω. For simplicity and proof of concept purposes, detector noises such as the shot noise and the thermal noise are neglected, therefore the noise seen in Fig. 2 arises from the phase and amplitude noises of the source used in our modeling. In the simulation, we use a 256μs time window with about 61 ps temporal resolution (i.e. 2^{22} samples), which corresponds to a total of a 16.4GHz frequency window and

Optics EXPRESS

~4kHz frequency resolution. The L_{ref} is preselected in the system as 10cm, and the target is set to be $L_m = 50$m away from the lidar with a movement speed of 30m/s (108km/h) in the direction of the laser beam propagation, and hence induces a 60MHz Doppler shift to the optical carrier at 1μm central wavelength [23]. Equations (2) and (3) are used by setting $\phi_o = \phi_i = 0$ to acquire the resultant I_{PD}. In practice, the initial phases of RF tones can be set by synchronization of RF generators via master-slave operation. The detected time-domain signal by the PD is converted into the RF spectrum via Fast Fourier Transform (FFT) as shown in Fig. 2. The significant frequencies at ω_d, ω_i, $2\omega_i$, $\omega_i \pm \omega_d$, and $2\omega_i \pm \omega_d$, are marked on the spectrum, while the resultant intermodulation tones that we don't utilize in our calculations remain unlabeled. There are in total of 8 frequency spikes that are applicable for Eq. (5). These peaks are found via a peak finding algorithm and by using the known ω_i and measured ω_d values as reference points.

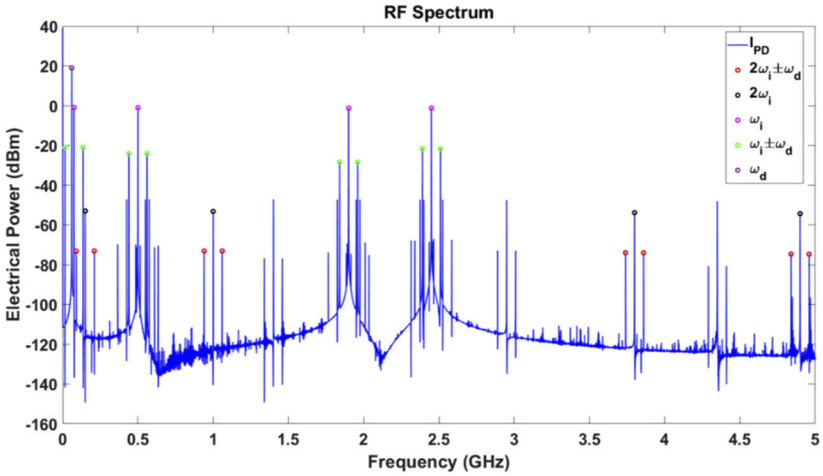

Fig. 2. RF spectrum of the resultant I_{PD} of a target at 50m with 108km/h speed. Each modulation tone, higher-order frequencies, their corresponding Doppler shifts, and the ω_d are indicated on the RF spectrum.

It is possible to acquire the value of ω_d by analyzing the spike near the baseband or the peaks near the known modulation tones in Fig. 2. The measured Doppler shift on the RF spectrum is 60MHz and the Doppler peak is indicated in Fig. 2 as ω_d. The resolution of the velocimetry is depending on the frequency resolution of the spectrum, $\delta\omega$. Therefore, the velocity resolution can be formalized by $\Delta v = (\pm\delta\omega/\omega_0)c$. In this particular simulation, the Δv of the MTCW system is 0.4cm/s due to the long time window. In the actual practice, there is an interplay between time window, i.e., velocimetry resolution, and the number of scans one can perform per second in most of the CW lidar systems, in particular FMCW lidar systems, which should be taken into account while configuring the lidar depending on the desired application.

The desired phases are extracted from the output voltage, V_{out}, or the generated photocurrent I_{PD}. After performing FFT, the resultant complex V_{out} yields the phase observed at that particular tone in between the interval of -π,π. This process can be further improved by using Bessel filters to generate the phases of individual tones. At this point, all the variables are found to compute L_m except for the value of n_i in Eq. (5). It is not possible to measure the exact number of complete cycles of a modulation tone via the MTCW methodology by looking at the results in a single tone. Hence a triangulation approach is used to generate the exact distance of the target using the individual $\omega_i \pm \omega_d$ phases. It is possible to further enhance the sensitivity of the methodology by employing $2\omega_i \pm \omega_d$ tones, however, these tones will have lower powers compared to $\omega_i \pm \omega_d$.

Optics EXPRESS

To find the measurement length, the possible n_i values are swept for each $\omega_i \pm \omega_d$. The highest n_i value belongs to the highest frequency tone with the smallest RF wavelength. The lowest frequency tone will have the lowest value of n_i. In an actual application, it is desired to have a minimum value of $n_i = 1$ within the maximum measurement range by selecting an appropriate tone frequency, or it is desired to use the time of arrival information of quasi-CW pulses to estimate a coarse range value. The calculated L_m results for the given n_i at the corresponding frequencies are shown in Fig. 3(a). Each frequency has a different repetition length of $2\pi c/(\omega_i \pm \omega_d)$ as the following, $L_{\omega_1-\omega_d}$ = 19.98m, $L_{\omega_1+\omega_d}$ = 2.22m, $L_{\omega_2-\omega_d}$ = 68.13cm, $L_{\omega_2+\omega_d}$ = 53.53cm, $L_{\omega_3-\omega_d}$ = 16.29cm, $L_{\omega_3+\omega_d}$ = 15.29cm, $L_{\omega_4-\omega_d}$ = 12.54cm and $L_{\omega_4+\omega_d}$ = 11.94cm.

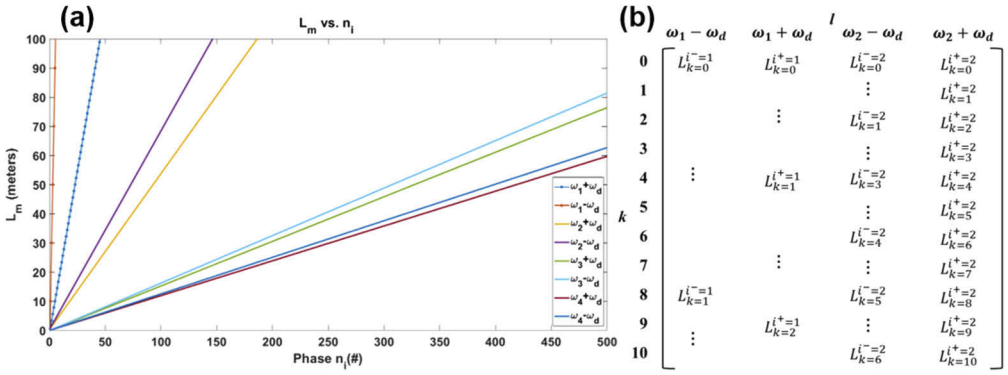

Fig. 3. (a) Measurement length results, $L_k^{\omega_i \pm \omega_d}$, after sweeping the n_i up to 500 for each $\omega_i \pm \omega_d$ (b) Representation of the first 11 rows of the $M_{k,l}$ matrix with 2 RF modulation tones with the calculated $L_k^{\omega_i \pm \omega_d}$ values. Blank spaces are repeating terms for k<10.

To estimate the actual L_m, first, we generate a data matrix $M_{k,l}$ such that $M_{k,l} = k(2\pi c/\omega_i \pm \omega_d) + L_0^{\omega_i \pm \omega_d}$, where $L_0^{\omega_i \pm \omega_d}$ is computed by using the equations in Table 1, $k = 1, 2, \ldots, n_{i-\max}$, and $l = 2N$. For illustration purposes, it is assumed that the measurement range we would like to resolve, L_{m-max}, is within $n_{i-max} = 500$ for the highest frequency tone. Since, for other lower frequencies, n_{i-max} will be lower for the same target range, we don't need to fill values of the matrix for the estimated length $L_k^i = k(2\pi c/\omega_i \pm \omega_d) + L_0 > L_{m-\max}$. Since $\omega_4+\omega_d$ will yield a better resolution due to its smaller repetition length, the last column of $M_{k,l}$ is set to the estimated L_m at each n_i, which will be used as the finest length resolution. The rest of the columns are filled in the same manner. However, range estimation values presented in new columns are selected in a manner to closely match the estimated L_m values in the last column. As the tone frequencies decrease, $2\pi c/(\omega_i \pm \omega_d)$ will repeat itself less often, hence we obtain repetitive terms in the previous columns, as illustrated in a sample matrix in Fig. 3(b).

After establishing the $M_{k,l}$, the standard deviation of each row is calculated and stored in the array σ_k as $\sigma_k = \sqrt{\frac{\sum_{i=1}^{l} (M_{k,i} - \overline{M_k})^2}{l}}$. Here, $\overline{M_k}$ stands for the mean of the k^{th} row. Then the last column of $M_{k,l}$ is matched with σ_k to find the standard deviation at the corresponding L_m. The length where the minimum σ_k is found will yield the closest target range. Figure 4 illustrates the σ values for a target at 50m away. The minimum σ_k corresponds to a target at $L_m = 50.0091$m that deviates 0.91cm from the actual. Here the error range is dictated by the time resolution δt of the detected signal as $\Delta L = (\pm \delta t \times c)/2$.

Detecting targets that are further than the λ_{RF-max} should be evaluated by considering the fact that the minimum standard deviation point repeats itself for every distance of $L_{rep} = 2\pi c/\omega_{gcd}$, where ω_{gcd} is the greatest common divisor of $\omega_i \pm \omega_d$ frequencies. In particular, for applications like aerial imaging or remote sensing through satellites or flying devices, a quasi-CW approach

Optics EXPRESS

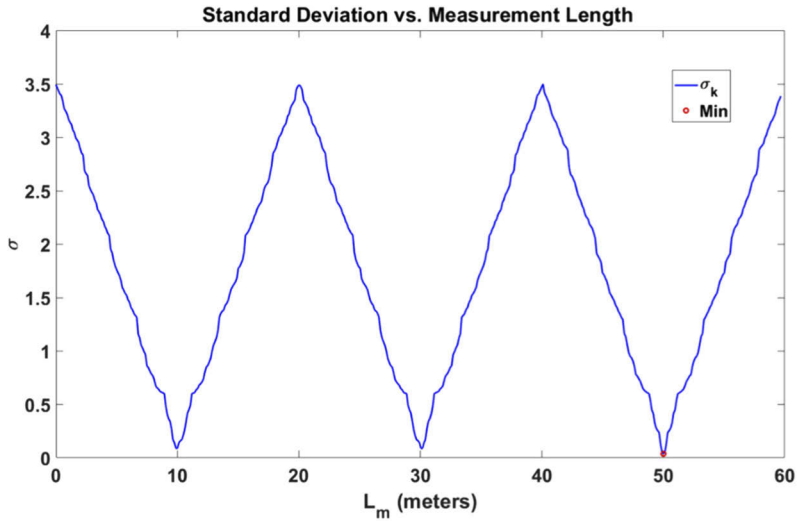

Fig. 4. σ_k with respect to L_m to find the distance of the target via triangulation. L_m set to 50m with a target speed of 108km/h. The minimum σ_k value is indicated in the figure.

should be utilized to generate long pulses with high peak power and RF modulations on top of them to mitigate the cyclic behavior. In such a method, the quasi-CW pulses offer the time of arrival measurements to capture coarse range measurements, while RF modulations on top of the long pulse facilitate more precise range and velocity measurements. Therefore, the span of n_i will be limited due to the time gating of the modulated pulses. At each interval, the selected n_i range will yield a single solution based on the measured tone frequencies and phases. In our theoretical model, L_{rep} is found to be ~60m, which corresponds to the greatest common divisor of all $\omega_i \pm \omega_d$ terms that is 5MHz. As a result, the minimum standard deviation repeats itself at 50m, 110m, 170m, ... etc. Hence, selecting tone frequencies in a way that the greatest common divisor of all $\omega_i \pm \omega_d$ terms is as small as possible will increase the $L_{rep.}$ Moreover, the quasi-CW pulsation and the considerate selection of the tone frequencies will prevent the potential false ranging measurements by eliminating additional close-to-minimum standard deviation points, which may occur due to the additional phase noise introduced by the lidar system. However, these calculations exclude the phase noise that might arise from the optical sources, detectors, RF generators, channel turbulences, and potential phase noise caused by the target surface roughness on the echo signal. Although the impact of the phase noise is left out for future study, in order to average the impact of phase noise, selection of tone frequencies can be engineered more carefully, and additional modulation tones can be added, if it is necessary, as a general principle.

4. Experimental verification

To prove the concept in the experimental domain, the test bench in [19] is used, i.e. the target in Fig. 1 is replaced by a reflector stationed on a translational motorized stage. The target is set to move with ~8cm/s and the 40cm long stage is placed 90cm away from the MTCW lidar. A region is selected on the stage for data acquisition that corresponds to a distance of 110-115cm from the detector since the actual distance of the target cannot be measured due to the movement of the target with an integrated PToF lidar for comparison and verification. The data is acquired while the target is moving through this predetermined location on the translational stage with a constant speed. A narrow linewidth 1550nm laser is modulated by 6 RF modulation tones are used at 79, 391, 971, 1657, 2159, and 2623MHz. An 8GHz bandwidth oscilloscope with a

Optics EXPRESS

20GSa/s sampling rate is used for data acquisition with a time window of 100μs and 50ps time resolution, and 10 kHz frequency resolution. The L_{ref} is measured to be 3cm and the initial tone phases, ϕ_i, are acquired from the E_{ref} spectrum to normalize the resultant $\omega_i \pm \omega_d$ phases. The triangulation algorithm is applied to the measured $\omega_i \pm \omega_d$ phases to compute the target distance. The velocity of the target is found using the RF peak near the baseband.

The final measured RF spectrum is presented in Fig. 5. Each ω_i and its corresponding $\omega_i \pm \omega_d$ are labeled on the spectrum as well as the Doppler frequency near the baseband. The measured Doppler spike is at 105kHz that is equal to 8.08cm/s at 1550nm with a ±0.8cm/s accuracy due to the frequency resolution of the measurement setup. For ranging, data matrix $M_{k,l}$ is generated by setting l to 12 and k to 30. The phase of $\omega_6 + \omega_d$ is used as the reference point to maximize resolution. The final σ_k and the minimum standard deviation point are shown in Fig. 6. The L_m is measured as 111.9cm that is within the predetermined measurement range. The expected ranging resolution, ΔL, is ±0.75cm based on the temporal resolution. The minimum σ_k is 0.15, where the minimum standard deviation should be zero in an ideal noiseless system. It is expected to have a nonzero standard deviation due to the noises. In particular, the laser phase noise, linewidth of the RF generators, and FFT leakage to side peaks caused broadening of ω_6 as shown in Fig. 6(b), which induces additional phase noise to the side peaks stationed at $\omega_6 \pm \omega_d$. Therefore, the measured value of the minimum σ_k is higher than the ideal case. However, since the same information is engraved into 12 different tones, averaging will mitigate the impact of the noise. As stated in the previous section a further study should be performed to quantify the impact of phase error on measurements more accurately.

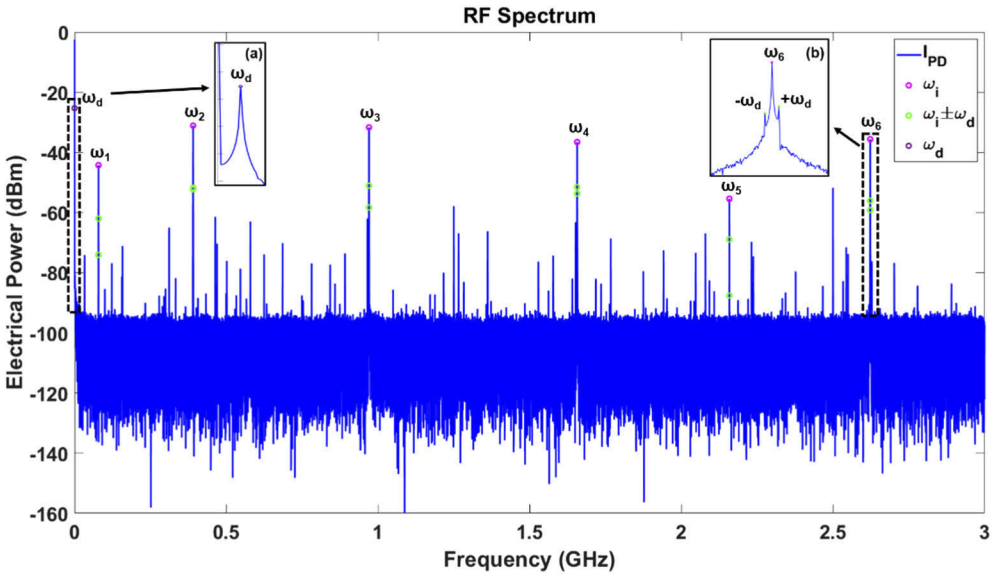

Fig. 5. Measured resultant RF spectrum of the target moving with ~8cm/s. 6 RF modulation frequencies are indicated on the spectrum. Insets (a) magnified Doppler spike near the baseband at 105kHz, (b) magnified ω_6 and its corresponding $\omega_6 \pm \omega_d$.

Optics EXPRESS

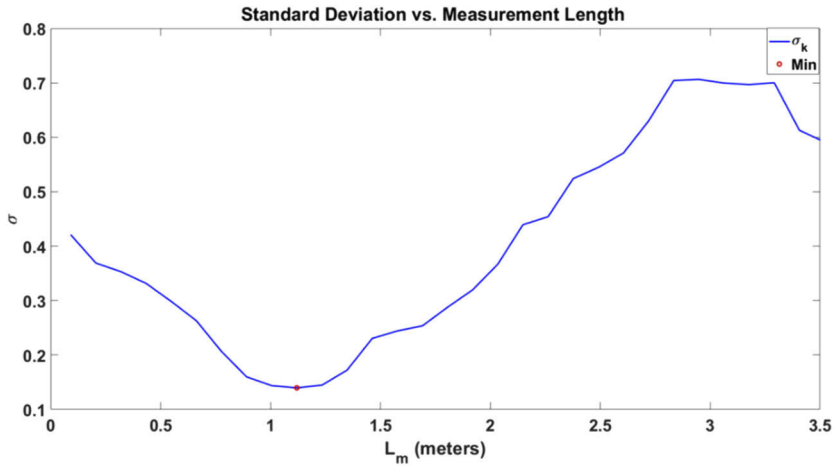

Fig. 6. σ_k with respect to L_m to find the distance of the target via triangulation. The minimum σ_k value is indicated in the figure at $L_m = 111.9$cm.

5. Conclusion

In this work, the enhancement of the MTCW lidar system to perform simultaneous ranging and velocimetry of moving targets is theoretically developed and demonstrated via numerical analysis and experimental results. Since the proposed approach uses a comparative analysis of narrowly spaced RF tones, it has the potential for eliminating the limits of the coherence length of lasers in lidar applications. For a numerical verification and explanation of the concept, a dummy target is assumed with 108km/h speed and 50m distance during the simulations. The target velocity is measured by evaluating the side peaks near the frequency tones. The acquired Doppler shift corresponds to the target's speed. Then by using the phase and measurement length relation at the individual $\omega_i \pm \omega_d$, the potential values are determined. A triangulation algorithm is built and used to extract the range of a target by utilizing the possible solutions of L_m at each frequency. The resolution of the velocimetry depends on the frequency resolution of the spectrum, while the ranging resolution is defined by the temporal resolution of detection electronics. In the presented simulations, the velocimetry and ranging resolutions are found to be ±0.4cm/s and ±1cm, respectively. Furthermore, the proposed concept is demonstrated in the experimental domain by using a dynamic target placed to a motorized translational stage. The target is measured to be at 111.9cm with 8.08cm/s speed by using the triangulation algorithm. By engineering the selected tone powers, detection electronics, and estimation algorithms, range and velocity resolution can be further improved for the proposed measurement technique.

Funding. Office of Naval Research (# N00014-18-1-2845).

Disclosures. The authors declare that there are no conflicts of interest related to this article.

References

1. J. Hecht, "Lidar for self-driving cars," Opt. Photonics News **29**(1), 26–33 (2018).
2. W. Zhang, "Lidar-based road and road-edge detection," in *IEEE Intelligent Vehicles Symposium* (IEEE 2010), pp. 845–848.
3. J. L. Bufton, J. B. Garvin, J. F. Cavanaugh, L. A. Ramos-Izquierdo, T. D. Clem, and W. B. Krabill, "Airborne lidar for profiling of surface topography," Opt. Eng. **30**(1), 72–79 (1991).
4. R. H. Couch, C. W. Rowland, K. S. Ellis, M. P. Blythe, C. R. Regan, M. R. Koch, C. W. Antill, W. L. Kitchen, J. W. Cox, and J. F. DeLorme, "Lidar In-Space Technology Experiment (LITE): NASA's first in-space lidar system for atmospheric research," Opt. Eng. **30**(1), 88–96 (1991).

Optics EXPRESS

5. P. Trocha, M. Karpov, D. Ganin, M. H. Pfeiffer, A. Kordts, S. Wolf, J. Krockenberger, P. Marin-Palomo, C. Weimann, and S. Randel, "Ultrafast optical ranging using microresonator soliton frequency combs," Science **359**(6378), 887–891 (2018).
6. M.-C. Amann, T. M. Bosch, M. Lescure, R. A. Myllylae, and M. Rioux, "Laser ranging: a critical review of unusual techniques for distance measurement," Opt. Eng. **40**(1), 10 (2001).
7. J. Liu, Q. Sun, Z. Fan, and Y. Jia, "TOF Lidar development in autonomous vehicle," in *IEEE Optoelectronics Global Conference* (IEEE, 2018), pp. 185–190.
8. J. Lee, Y.-J. Kim, K. Lee, S. Lee, and S.-W. Kim, "Time-of-flight measurement with femtosecond light pulses," Nat. Photonics **4**(10), 716–720 (2010).
9. S. Schuon, C. Theobalt, J. Davis, and S. Thrun, "Lidarboost: Depth superresolution for tof 3d shape scanning," in *IEEE Conference on Computer Vision and Pattern Recognition* (IEEE, 2009), pp. 343–350.
10. M. U. Piracha, D. Nguyen, I. Ozdur, and P. J. Delfyett, "Simultaneous ranging and velocimetry of fast moving targets using oppositely chirped pulses from a mode-locked laser," Opt. Express **19**(12), 11213–11219 (2011).
11. P. F. McManamon, *LiDAR Technologies and Systems* (SPIE Press, Bellingham, WA, 2019).
12. A. D. Payne, A. A. Dorrington, M. J. Cree, and D. A. Carnegie, "Improved measurement linearity and precision for AMCW time-of-flight range imaging cameras," Appl. Opt. **49**(23), 4392–4403 (2010).
13. R. D. Peters, O. P. Lay, S. Dubovitsky, J. P. Burger, and M. Jeganathan, "MSTAR: an absolute metrology sensor with sub-micron accuracy for space-based applications," in *Proc. SPIE* 10568, p. 105682O-1.
14. N. R. Newbury, "Searching for applications with a fine-tooth comb," Nat. Photonics **5**(4), 186–188 (2011).
15. R. Agishev, B. Gross, F. Moshary, A. Gilerson, and S. Ahmed, "Range-resolved pulsed and CWFM lidars: potential capabilities comparison," Appl. Phys. B **85**(1), 149–162 (2006).
16. Z. W. Barber, W. R. Babbitt, B. Kaylor, R. R. Reibel, and P. A. Roos, "Accuracy of active chirp linearization for broadband frequency modulated continuous wave ladar," Appl. Opt. **49**(2), 213–219 (2010).
17. R. Torun, M. M. Bayer, I. U. Zaman, and O. Boyraz, "Multi-tone modulated continuous-wave lidar," in *Proc. SPIE 10925*, Vol. 10925, p. 109250 V.
18. R. Torun, M. M. Bayer, I. U. Zaman, J. E. Velazco, and O. Boyraz, "Realization of Multitone Continuous Wave Lidar," IEEE Photonics J. **11**(4), 1–10 (2019).
19. M. M. Bayer, R. Torun, X. Li, J. E. Velazco, and O. Boyraz, "Simultaneous ranging and velocimetry with multi-tone continuous wave lidar," Opt. Express **28**(12), 17241–17252 (2020).
20. M. M. Bayer, R. Torun, I. U. Zaman, and O. Boyraz, "A Basic Approach for Speed Profiling of Alternating Targets with Photonic Doppler Velocimetry," in *Conference on Lasers and Electro-Optics, OSA Technical Digest* (Optical Society of America, 2019), p. AW4 K.4.
21. O. Boyraz, M. M. Bayer, R. Torun, and I. Zaman, "Multi Tone Continuous Wave Lidar (Invited)," in 2019 IEEE Photonics Society Summer Topical Meeting Series (SUM) (2019), pp. 1–2.
22. Q. Chen, "Airborne lidar data processing and information extraction," Photogramm. Eng. Rem. S. **73**, 109 (2007).
23. D. H. Dolan, "Accuracy and precision in photonic Doppler velocimetry," Rev. Sci. Instrum. **81**(5), 053905 (2010).
24. O. T. Strand, D. R. Goosman, C. Martinez, T. L. Whitworth, and W. W. Kuhlow, "Compact system for high-speed velocimetry using heterodyne techniques," Rev. Sci. Instrum. **77**(8), 083108 (2006).
25. Z. Xu, L. Tang, H. Zhang, and S. Pan, "Simultaneous real-time ranging and velocimetry via a dual-sideband chirped lidar," IEEE Photonic Tech. L. **29**(24), 2254–2257 (2017).